Ferric *trans*-1,2-Diaminocyclohexanetetraacetic Acid ($Fe^{3+}CDTA^{4-}$/$Fe^{3+}OH^{-}CDTA^{4-}$) in NaCl Aqueous Solutions: Effect of Temperature on the Hydroxy Complex Formation Thermodynamic Constant and on the Activity Coefficient Ion-Interaction Parameters

Simon Piché and Faïçal Larachi*

Department of Chemical Engineering, Laval University, Ste-Foy, Canada PQ G1K 7P4

The impact of the variation of temperature from (280 to 323) K on the thermodynamic equilibrium constant ($K°$) for the $Fe^{3+}CDTA^{4-} + OH^- \rightleftarrows Fe^{3+}OH^-CDTA^{4-}$ complex formation reaction (CDTA is *trans*-1,2-diaminocyclohexanetetraacetic acid) was investigated in alkaline solutions. $K°$ is obtained by multiplying the equilibrium reaction product (K_m) measured from species molal concentrations by the activity coefficient quotient ($\gamma_\pm$) predicted by either the Hückel, Bromley, Scatchard, or Pitzer models, all of which required knowledge of ion-interaction empirical constants. For each temperature set at (280, 288, 298, 305, 313, 323) K ± 1 K, the measured K_m values acquired for a multitude of sodium chloride solutions of (1.5×10^{-4} to 0.95) mol kg^{-1} were fitted on the ($K°/\gamma_\pm$) relationship for all four activity coefficient models. $K°$ and ion-interaction empirical constants were obtained from this action. $K°$ values computed from the six temperature sets were used to evaluate the reaction enthalpy ($\Delta_r H_m$) and entropy ($\Delta_r S_m$) associated with the above complex formation reaction. $\Delta_r H_m$ was estimated to be (−17.7 ± 0.5) kJ mol^{-1}, whereas $\Delta_r S_m$ was fixed at 23.0 J mol^{-1} K^{-1}. It was also determined that most of the models ion-interaction empirical constants do not change with temperature in a recognizable way within the studied range. The only exception involves Pitzer's ion-interaction summations ($\Sigma\beta^0_\pm$, $\Sigma\beta^1_\pm$) where a slight but definite trend was observed in relation to temperature.

Introduction

Ferric chelates (e.g., ferric *trans*-1,2-diaminocyclohexanetetraacetate, $Fe^{3+}CDTA$;[4−] ferric ethylenediaminotetraacetate, $Fe^{3+}EDTA^{4-}$) are already in use as redox catalysts for the removal of hydrogen sulfide (H_2S) contained in sour gas streams including natural gas.[1−5] Hydrogen sulfide is also part of a vast environmental problem afflicting pulp mills that use the Kraft process. Current abatement processes such as gas incineration, chemical oxidation, and alkaline/amine scrubbing are used to prevent H_2S and other reduced sulfur compounds (i.e., CH_3SH, $(CH_3)_2S$, $(CH_3)_2S_2$) from release into the atmosphere because they are responsible for unpleasant odors in the neighborhood. Although mostly efficient, high costs (i.e., incinerator, chemical oxidizer) and resulting environmental predicaments (i.e., SO_2 emission, chlorinated byproducts) reveal the complexity of the problem for which the best solution must converge toward high H_2S/reduced sulfur removal per invested dollar. With the prospect of stricter regulations on reduced sulfur emissions, Iliuta and Larachi[6] demonstrated the possibilities of a bifunctional redox process where a ferric chelate (i.e., $Fe^{3+}CDTA^{4-}$) is used to throttle H_2S emissions (eq 1) while dissolved oxygen regenerates the ferrous chelate product into the active ferric form (eq 2). Both reactions are performed simultaneously within the same scrubbing device.

$$H_2S_{(aq)} + 2Fe^{3+}CDTA^{4-} + 2OH^- \rightarrow S^0 + 2Fe^{2+}CDTA^{4-} + 2H_2O \quad (1)$$

$$2Fe^{2+}CDTA^{4-} + 0.5O_2 + H_2O \rightarrow 2Fe^{3+}CDTA^{4-} + 2OH^- \quad (2)$$

To follow up such a program, the composition of the reactive solution must be looked at with great care. For instance, alkaline conditions are propitious to accelerate gaseous H_2S absorption to generate hydrosulfides (HS^-) following aqueous H_2S dissociation ($pK_a = 7.1$ at 298 K). Under such conditions, a hexadentate ligand such as CDTA with four oxygen and two nitrogen donors matching the coordination number of iron will form highly stable $Fe^{3+}CDTA$.[4−7,8] However, this species can evolve into a seven-coordinate structure ($Fe^{3+}OH^-CDTA^{4-}$) due in part to steric considerations associated with the ligand.[9] Both species coexist in equilibrium depending on the aqueous environment characterized by pH, temperature, ionic strength, and electrolyte composition.

$$Fe^{3+}CDTA^{4-} + OH^- \rightleftarrows Fe^{3+}OH^-CDTA^{4-} \quad (3)$$

Careful knowledge of $Fe^{3+}CDTA^{4-}$ and $Fe^{3+}OH^-CDTA^{4-}$ concentrations is of utmost importance because each Fe(III) species is thought to possess highly contrasting reactivity toward hydrosulfides. In previous work,[10] the thermodynamic equilibrium constant for the hydroxy complex formation of ferric CDTA ($K°$) was evaluated at 298 ± 1 K using a variety of aqueous environments consisting of sodium chloride, sodium sulfate, or lithium chloride

* To whom inquiries should be directed. E-mail: faical.larachi@gch.ulaval.ca. Tel: 1-418-656-3566. Fax: 1-418-656-5993.

10.1021/je049647f CCC: $30.25
Published on Web 03/01/2005

Table 1. Temperature-Dependent Water Dissociation Constant (K_w),[20] Water Density (ρ_w), and Debye−Hückel Constant (A_ϕ)[19]

T/K	K_w	ρ_w/kg dm^{-3}	A_ϕ/kg$^{-0.5}$ mol$^{-0.5}$
280	0.24×10^{-14}	1.000	0.495
288	0.45×10^{-14}	0.999	0.502
298	1.00×10^{-14}	0.998	0.509
305	1.72×10^{-14}	0.995	0.517
313	2.92×10^{-14}	0.992	0.524
323	5.47×10^{-14}	0.988	0.534

electrolytic solutions. $K°$ was obtained by multiplying the measured equilibrium reaction product (K_m) with the activity coefficient quotient ($\gamma_\pm$) predicted by the Hückel,[11,12] Bromley,[11,13,14] Scatchard,[12,15,16] and Pitzer[11,17−19] models.

$$K° = \left(\frac{\gamma_{s2}}{\gamma_{s1}\gamma_{OH^-}}\right)\left(\frac{m_{s2}}{m_{s1}m_{OH^-}}\right) = \gamma_\pm K_m \qquad (4)$$

in which s1 and s2 stand for $Fe^{3+}CDTA^{4-}$ and $Fe^{3+}OH^-$-$CDTA,^{4-}$ respectively. K_m was measured from species molal concentrations (m_{s2}, m_{s1}, m_{OH-}) for a multitude of ionic strengths $I_m = (1.5 \times 10^{-4}$ to 1.8) mol kg^{-1}. However, the variation of the solution density (ρ) was neglected in this earlier study, so the equilibrium species molarity was used instead of molality (i.e., $m_{s1} \equiv c_{s1}$; $K_m \equiv K_c$). In the present work, K_m was calculated using the pH, species molar concentrations (c_{s1}, c_{s2}), knowledge of the water dissociation constant at a given temperature (K_w), and estimation of the solution density (eqs 5 and 6).

$$K_m = \frac{m_{s2}}{m_{s1}}\frac{\gamma_{H^+}\gamma_{OH^-}m_{H^+}}{K_w} = \frac{c_{s2}}{c_{s1}}\frac{10^{-pH}}{K_w\rho} = \frac{K°}{\gamma_{OH^-}\gamma_\pm} \qquad (5)$$

$$\rho = \rho_w + 0.0585c_{NaCl} \qquad (6)$$

where ρ_w/kg dm^{-3} is the density of pure water at given temperature and $0.0585c_{NaCl}$ accounts for NaCl density correction. The implicit effect of ionic strength on hydroxide activity (γ_{OH^-}) was not directly calculated but rather lumped into the overall activity coefficient quotient ($\gamma_\pm \equiv \gamma_{OH^-}\gamma_\pm$). K_w and ρ_w values, being functions of temperature, are given in Table 1.[20]

In the present work, the thermodynamic equilibrium constant ($K°$) for the hydroxy complex formation reaction (eq 3) was evaluated for every studied temperature at $T =$ (280, 288, 298, 305, 313, 323) K on the basis of several K_m measurements obtained in a multitude of sodium chloride solutions of (1.5×10^{-4} to 0.95) mol kg^{-1}. This was achieved in conjunction with predictions of the activity coefficient quotient ($\gamma_\pm$) using the four models, all of which require a knowledge of ion-interaction empirical constants. For each temperature set, simultaneous fitting of $K°$ with the empirical constants was performed on K_m measurements. Then, $K°$ values computed from the six temperature sets were used to evaluate the reaction enthalpy ($\Delta_r H_m$) and entropy ($\Delta_r S_m$) associated with the above complex-formation reaction. The effect of temperature on the ion-interaction empirical constants for each model was also assessed.

Experimental Section

The equilibrium experiments were conducted in a hybrid aluminum/Plexiglas stirred cell of 12.7 cm i.d. and 25.4 cm height (Figure 1). The lower section made of aluminum (12.7 cm high) containing the experimental solution was in direct contact with the heat-exchanging water bath outside the stirred cell. The upper section made of Plexiglas (12.7 cm high) with its low thermal conductivity prevented important energy loss from the gas phase and thus allowed better control over the solution temperature. Radial and axial six-bladed turbine stirrers (6.35 cm i.d.) were centrally located in the stirred cell plunging into the solution at distances of 2.5 cm (axial stirrer) and 5 cm (radial stirrer) from the bottom. Four symmetrically mounted baffles increased the stirring efficiency and prevented vortex formation.

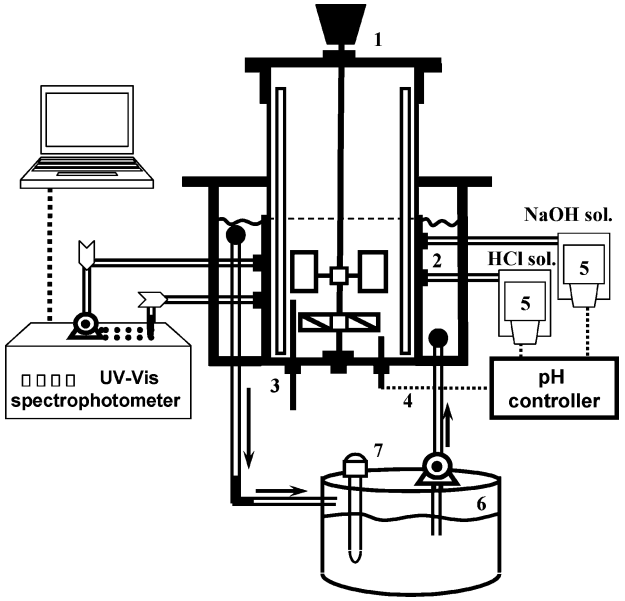

Figure 1. Stirred cell reactor with appendices: 1, rotor; 2, makeup acid and base inlet; 3, thermistor; 4, pH probe; 5, volumetric pumps; 6, heating/cooling water tank; 7, immersion heater.

Ferric CDTA stock solutions were prepared following the same recipe described previously[10] with a final concentration of $(38.5 \pm 0.6) \times 10^{-3}$ mol dm^{-3} and a pH approaching 4. Overall, (6 ± 0.06) cm^3 of the stock solution was added to (1500 ± 15) cm^3 of a NaCl electrolytic solution of specified ionic strength ranging between 1.5×10^{-4} and 0.95 mol kg^{-1}. This led to a diluted ferric CDTA concentration of $(0.150 \pm 0.002) \times 10^{-3}$ mol dm^{-3}, which was fed to the stirred cell. Before each trial, a 25 L water reservoir was preheated to the experimental temperature of $T =$ (305, 313, 323) K with an immersion heater while its contents were pumped into the heat-exchanging bath and recycled back into the reservoir (Figure 1). Ice was used to regulate cooler temperatures, $T =$ (280, 288) K. The measurements began only when the NaCl/$Fe^{3+}CDTA^{4-}$ solution temperature was attained and controlled to within ±1 K. Then, a sequence of six to seven different Fe^{3+}-$CDTA^{4-}$/$Fe^{3+}OH^-CDTA^{4-}$ concentration distributions was obtained by varying the temperature-corrected pH anywhere between 8.05 ± 0.05 and 10.55 ± 0.05. This was achieved via a pH controller (Liquitron DP5000, LMI Milton Roy) connected to a Cole-Parmer in-line activity probe inserted into the cell. NaOH and HCl solutions of (0.1 ± 0.002) mol dm^{-3} were employed for pH control. After the required pH was attained, a sample of the investigated solution was extracted from the stirred cell via a peristaltic pump (Varian routine sampler accessory) and rerouted to the spectrophotometer (Varian Cary 300 model) in-line cavity for reading in the (225 to 325) nm band. $Fe^{3+}CDTA^{4-}$ and $Fe^{3+}OH^-CDTA^{4-}$ species generate different UV absorbance spectra in this region. Spectral quantitative processing was achieved using PLSplus IQ principle com-

Table 2. Averaged Equilibrium Reaction Product[a] for the $Fe^{3+}CDTA/Fe^{3+}OH^{-}CDTA$ Pair in NaCl Aqueous Solutions Maintained at Various Temperatures and Ionic Strengths

	T/K				
I_c/mol dm^{-3}[b]	280	288	305	313	323
(1.78 to 3.94) × 10^{-4}[c]	4.458 ± 0.061	4.434 ± 0.031	4.236 ± 0.032	4.094 ± 0.025	4.07 ± 0.057
(7.66 to 9.72) × 10^{-4}[c]	4.457 ± 0.035		4.200 ± 0.049	4.077 ± 0.043	
(2.32 to 2.58) × 10^{-3}[c]	4.428 ± 0.024	4.416 ± 0.038	4.145 ± 0.047	4.083 ± 0.037	4.058 ± 0.055
0.0103 ± 0.0002	4.410 ± 0.031	4.348 ± 0.029	4.121 ± 0.045	4.009 ± 0.034	4.011 ± 0.038
0.0255 ± 0.0005	4.381 ± 0.033	4.300 ± 0.022	4.113 ± 0.035	4.045 ± 0.029	3.998 ± 0.032
0.0502 ± 0.001	4.369 ± 0.022	4.305 ± 0.023	4.125 ± 0.036	4.037 ± 0.023	3.962 ± 0.029
0.0753 ± 0.0015	4.390 ± 0.016		4.137 ± 0.026	4.041 ± 0.037	
0.1 ± 0.002	4.403 ± 0.031	4.355 ± 0.028	4.136 ± 0.052	4.052 ± 0.027	3.973 ± 0.022
0.15 ± 0.003	4.440 ± 0.028		4.205 ± 0.017	4.101 ± 0.062	4.035 ± 0.029
0.2 ± 0.004	4.455 ± 0.036	4.420 ± 0.025	4.195 ± 0.042	4.126 ± 0.027	4.055 ± 0.027
0.25 ± 0.005	4.492 ± 0.028		4.249 ± 0.024	4.164 ± 0.033	4.089 ± 0.031
0.35 ± 0.007	4.518 ± 0.035	4.502 ± 0.028	4.278 ± 0.045	4.205 ± 0.022	4.253 ± 0.042
0.5 ± 0.01	4.589 ± 0.044		4.328 ± 0.029	4.346 ± 0.027	4.390 ± 0.028
0.6 ± 0.012	4.641 ± 0.038	4.563 ± 0.012	4.330 ± 0.036	4.398 ± 0.030	
0.75 ± 0.015	4.626 ± 0.033	4.636 ± 0.028	4.412 ± 0.020	4.466 ± 0.039	4.514 ± 0.027
1.0 ± 0.02	4.697 ± 0.028	4.685 ± 0.013	4.507 ± 0.038	4.643 ± 0.027	4.625 ± 0.048

[a] $\log_{10} K_m$ ± std deviation of five to seven values. [b] Ionic strength values are given as NaCl molar concentration values (I_c) except for cases involving a range where no NaCl was added. In $\gamma_\pm$ calculations, I_m/mol kg^{-1} was used. [c] Presence of an ionic strength range is due to the addition of NaOH solution for pH adjustment.

Table 3. Best Fitted log *K*° and Activity Coefficient Models Parameters[a]

	T/K					
	280	288	298	305	313	323
Hückel equation						
log *K*°	4.487	4.428	4.258	4.225	4.122	4.087
log *K*° + log K_w	−10.316	−9.916	−9.742	−9.539	−9.412	−9.175
ϵ/kg mol^{-1}	1.397	1.510	2.293	1.528	1.663	1.511
AAE ($0 < I_m < 0.25$ mol kg^{-1})	0.024	0.027	0.039	0.034	0.031	0.030
Bromley model						
log *K*°	4.506	4.450	4.308	4.240	4.119	4.080
log *K*° + log K_w	−10.117	−9.894	−9.692	−9.525	−9.416	−9.182
B_1/mol kg^{-1}	1.751	1.819	1.976	1.824	2.004	2.047
B_2	2.587	2.707	2.630	2.647	2.646	2.635
AAE ($0 < I_m < 0.95$ mol kg^{-1})	0.033	0.030	0.060	0.036	0.029	0.039
Scatchard expansion						
log *K*°	4.474	4.420	4.277	4.223	4.111	4.070
log *K*° + log K_w	−10.150	−9.924	−9.723	−9.542	−9.424	−9.192
C_1/kg mol^{-1}	−1.606	−1.670	−2.092	−1.573	−1.763	−1.756
C_2/kg^2 mol^{-2}	1.742	1.821	1.867	1.737	1.627	1.590
C_3/kg^3 mol^{-3}	−0.784	−0.840	−0.636	−0.879	−0.847	−0.836
AAE ($0 < I_m < 0.95$ mol kg^{-1})	0.026	0.024	0.039	0.033	0.028	0.040
Pitzer model						
log *K*°	4.491	4.437	4.261	4.239	4.130	4.092
log *K*° + log K_w	−10.133	−9.907	−9.739	−9.526	−9.404	−9.170
$\Sigma\beta^0_\pm$	−0.280	−0.291	−0.345	−0.417	−0.912	−0.973
$\Sigma\beta^1_\pm$	−4.202	−4.347	−6.265	−4.302	−3.648	−3.583
β^1_{salt}	−2.486	−2.497	−4.577	−2.938	−2.744	−2.435
AAE ($0 < I_m < 0.95$ mol kg^{-1})	0.026	0.026	0.037	0.034	0.029	0.040
av of log *K*°	4.490	4.434	4.276	4.232	4.121	4.082
std deviation of log *K*°	0.013	0.013	0.013	0.009	0.008	0.010

[a] AAE is the average absolute error for the equilibrium reaction product.

ponent regression (PCR) analysis from Thermo Galactic Grams/32 AI software according to calibration sets described in previous work.[10]

Equilibrium Reaction Product (K_m)

Spectral analysis of the aqueous solution for each T, I_m, pH combination set led to the evaluation of individual $Fe^{3+}CDTA^{4-}$ and $Fe^{3+}OH^{-}CDTA^{4-}$ concentrations and therefore the calculation of K_m values according to eq 5. Table 2 presents log K_m as a characteristic average of the five to seven measurements taken at different pH values. Values for the 298 K set are given in Piché et al.[10]

Activity Coefficients Modeling ($\gamma_\pm$)

Alternatives for computing activity coefficients ($\gamma_\pm$) were scrutinized in the previous study. First, Hückel adjusted the extended Debye−Hückel limiting law (eq 7) by adding a term ($-\epsilon I_m$) accounting for increasing ion−ion interactions at higher ionic strengths, I_m = (0.1 to 0.25) mol kg^{-1}. Otherwise ($I_m < 0.1$ mol kg^{-1}), the extended Debye−Hückel equation holds properly. Newly fitted salting-out constants (ϵ) in conjunction with thermodynamic constants (log *K*°) for individual temperature sets are given in Table 3 along with the quality of fit (i.e., AAE, average absolute error). This includes a reassessment of the 298 K set ($I_m \leq 1$ mol kg^{-1}) published earlier.

$$\log_{10}\gamma_\pm = \frac{A_\phi \Delta z^2 \sqrt{I_m}}{1 + \beta\sqrt{I_m}} \qquad (7)$$

A_ϕ, defined as the Debye−Hückel constant, is temperature-

dependent[19] (Table 1), whereas $\Delta z^2 = 2$ and β is simplified to unity. The best $\log K^\circ - \log \gamma_\pm$ correspondence over $\log K_m$ was also achieved using Bromley (eq 8) and Pitzer (eq 9) models as well as the Scatchard (eq 10) power series expansion, all relevant to NaCl solutions. Accordingly, empirically fitted parameters that are said to be temperature-dependent[11] are displayed in Table 3 (Bromley: B_1, B_2; Pitzer: $\Sigma\beta^0_\pm$, $\Sigma\beta^1_\pm$, β^1_{salt}; Scatchard: C_1, C_2, C_3).

$$\log_{10}\gamma_\pm = \frac{A_\phi \Delta z^2 \sqrt{I_m}}{1+\sqrt{I_m}} - B_1 I_m + \frac{(0.06 - 0.6B_1)\Delta z^2}{(1 + 3I_m/2\Delta z^2)^2} I_m + B_2\sqrt{I_m}\{1 - \exp(-\sqrt{I_m})\} \quad (8)$$

$$\log_{10}\gamma_\pm = \frac{A_\phi \Delta z^2}{\ln 10}\left(\frac{\sqrt{I_m}}{1+1.2\sqrt{I_m}} + \frac{5}{3}\ln(1+1.2\sqrt{I_m})\right) + \frac{2I_m}{\ln 10}\{\sum\beta^0_\pm + \beta^1_{\text{salt}}\exp(-2\sqrt{I_m})\} + \frac{\sum\beta^1_\pm - \beta^1_{\text{salt}}}{\ln 10}\{1 - (1+2\sqrt{I_m})\exp(-2\sqrt{I_m})\} \quad (9)$$

$$\log_{10}\gamma_\pm = \frac{2.344}{\ln 10}\left(\frac{\sqrt{I_m}}{1+1.5\sqrt{I_m}}\right) + C_1 I_m + C_2 {I_m}^2 + C_3 {I_m}^3 \quad (10)$$

A demonstration of $\log K_m$ dispersion around Pitzer predictions is shown in Figure 2. Although several cases present seemingly large deviations within an experimental set, $-\log \gamma_\pm$ (i.e., Pitzer model) predictions still generate satisfactory fitting discrepancies within the accepted limits of AAE < 0.05 on $\log K_m$. The scattering is mainly the result of difficulties in controlling the solution's pH, which could be set only within a specified range of ±0.05. In addition, the possible spectral, temperature, and general experimental errors should explain the extent of $\log K_m$ scattering.

Figure 2 clearly illustrates that $\log K^\circ$ at $I_m \rightarrow 0$ decreases with increasing temperature. For that reason, an exothermic reaction enthalpy ($\Delta_r H_m$) is to be expected on the basis of the reaction given in eq 3. By relating $\ln K^\circ$ values as a function of inverse temperature (Figure 3), $\Delta_r H_m$ was evaluated to be (−17.8 ± 0.5) kJ mol^{-1} (−2146R/1000) allowing an entropy of formation ($\Delta_r S_m$) of 22.5 J mol^{-1} K^{-1} (2.704R). In a similar study, Gustafson and Martell[21] estimated $\Delta_r H_m$ and $\Delta_r S_m$ from potentiometric titration experiments to be (41.9 ± 0.8) kJ mol^{-1} and −37.7 J mol^{-1} K^{-1}, respectively, for the following equilibrium: Fe^{3+} + $CDTA^{4-}$ + $H_2O \rightleftharpoons Fe^{3+}OH^-CDTA^{4-} + H^+$. Calculation of the thermodynamic constants for the latter complex reaction was achieved in our database with the application of eq 11. By comparison with eq 5 and knowing that $\gamma_\pm$ does not transform, a new constant was obtained as $K^\circ_{\text{eq 11}} = K^\circ_{\text{eq 5}} K_w$ (Table 3). Recalculation of the reaction enthalpy and entropy based on $K^\circ_{\text{eq 11}}$ gives $\Delta_r H_m$ = (37.9 ± 0.5) kJ mol^{-1} and $\Delta_r S_m$ = −58.7 J mol^{-1} K^{-1}, which roughly correspond to the values obtained by Gustafson and Martell.

$$K^\circ = \gamma_\pm \frac{c_{s2}}{c_{s1}} \frac{10^{-\text{pH}}}{\rho} \quad (11)$$

K° and $\gamma_\pm$ Normalization

A quick assessment of modeled $\gamma_\pm$ ion-interaction parameters (i.e., ϵ, B_1, and B_2; see Table 3) reveals that temperature does not influence such parameters to a great extent, at least within the studied temperature range of (280 to 323) K. This behavior complies with Pitzer's affirmation that very little change in its model parameters

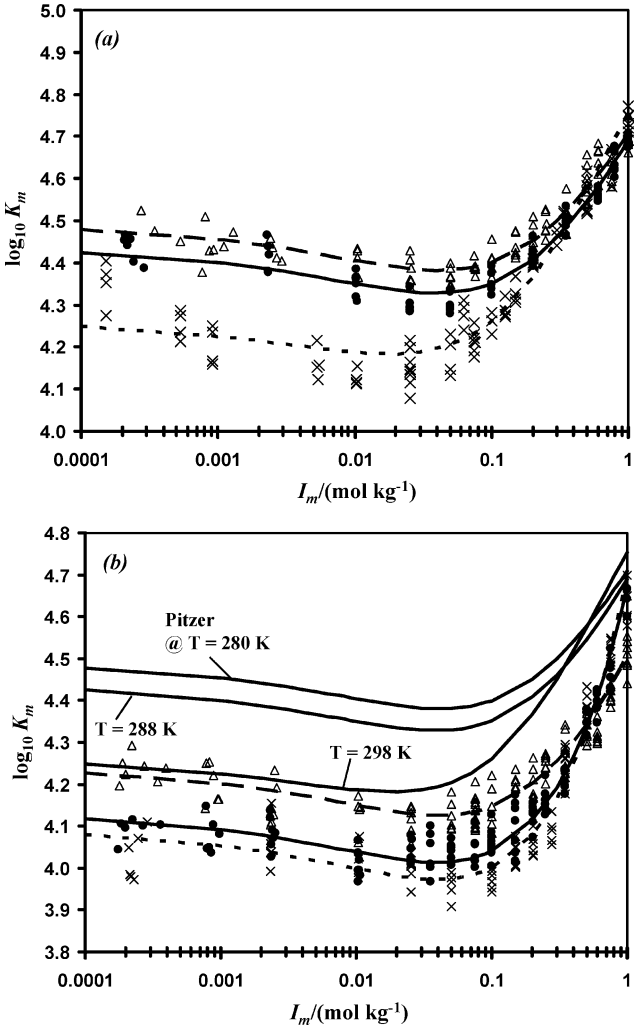

Figure 2. Experimental $\log K_m$ as a function of ionic strength (I_m) for NaCl solutions maintained at (a) Δ, 280 K; ●, 288 K; ×, 298 K and (b) △, 305 K; ●, 313 K; ×, 323 K (curves correspond to K_m predictions according to Pitzer's activity coefficient model).

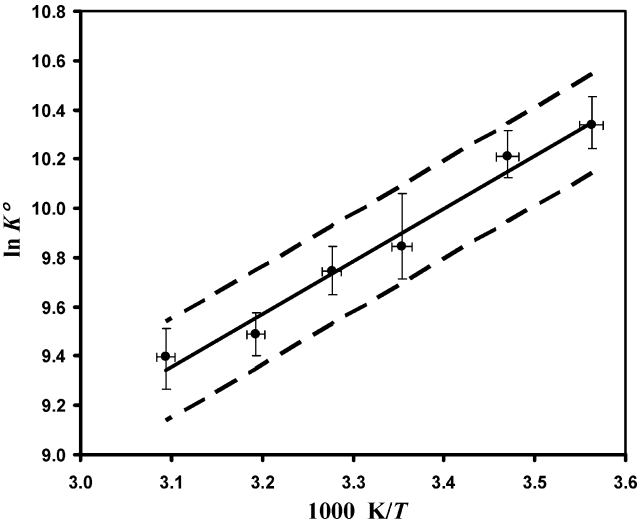

Figure 3. $\ln K^\circ$ against 1000 K/T schematic plot based on averaged K° values from all four activity coefficient models. Best fit: $\ln K^\circ$ = 2146 K/T + 2.704. (Dotted lines correspond to the experimental inaccuracy).

Table 4. Ion-Interaction Constants Average and the Consequence of Their Application in the Model for the Average Absolute Error (AAE)

	T/K					
	280	288	298	305	313	323
Hückel equation: $\epsilon = (1.650 \pm 0.326)$ kg mol^{-1}						
AAE	0.034	0.029	0.067	0.036	0.031	0.032
AAE − $AAE_{Tab.3}$	+0.010	+0.002	+0.028	+0.002	0	+0.002
Bromley model: $B_1 = (1.903 \pm 0.120)$ mol kg^{-1}, $B_2 = (2.642 \pm 0.038)$						
AAE	0.065	0.059	0.070	0.052	0.052	0.071
AAE − $AAE_{Tab.3}$	+0.022	+0.029	+0.010	+0.016	+0.023	+0.032
Scatchard expansion: $C_1 = (-1.743 \pm 0.187)$ kg mol^{-1}, $C_2 = (1.730 \pm 0.107)$ kg^2 mol^{-2}, $C_3 = (-0.804 \pm 0.088)$ kg^3 mol^{-3}						
AAE	0.051	0.047	0.073	0.052	0.040	0.065
AAE − $AAE_{Tab.3}$	+0.025	+0.023	+0.034	+0.019	+0.012	+0.025

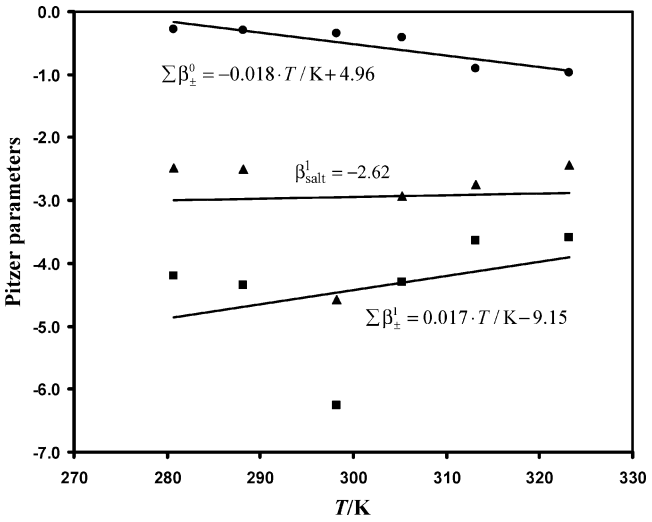

Figure 4. Evolution of Pitzer's ion interaction summations ($\Sigma\beta^0_{\pm}$, $\Sigma\beta^1_{\pm}$, β^1_{salt}) with temperature.

over the (298 to 573) K temperature range should be detected.[11] This observation is especially true for the Hückel, Bromley, and Scatchard models where no specific trend was observed. Their fitting parameters averaged over the six temperature sets are given in Table 4. Inclusion of these averages into $\gamma_{\pm}$ models instead of the individually adjusted parameter values confirms that one value for each ion-interaction parameters is sufficient to describe the whole (280 to 323) K temperature range. Despite an obvious inflation in the calculation error after normalization, the shift in prediction remains within acceptable limits with a maximum AAE increase of +0.034 leaking from the Scatchard expansion at 298 K (Table 4). However, temperature minimally influences Pitzer ion-interaction summations as shown in Figure 4. Although marginal, $\Sigma\beta^0_{\pm}$ and $\Sigma\beta^1_{\pm}$ exhibit a linear dependence on temperature, and β^1_{salt} can be considered to be constant over the (280 to 323) K range. Accordingly, normalization of the Pitzer model over the entire database was performed by simultaneously fitting $\Sigma\beta^0_{\pm}$ (as $\Sigma\beta^0_{\pm S}T + \Sigma\beta^0_{\pm I}$), $\Sigma\beta^1_{\pm}$ (as $\Sigma\beta^1_{\pm S}T + \Sigma\beta^1_{\pm I}$) and β^1_{salt} together with optimized $\Delta_r H_m$ and $\Delta_r S_m$ values through eq 12. Subscripts I and S represent the intercept and slope of the linearization.

$$\log_{10} K^\circ = \frac{1}{2.303}\left(\frac{-\Delta_r H_m}{R}\frac{1}{T} + \frac{\Delta_r S_m}{R}\right) \qquad (12)$$

Final normalization of the Pitzer model on the studied complex-formation reaction is represented in Table 5. Generally, little optimization was needed, although it was necessary to homogenize the data sets. The reaction enthalpy ($\Delta_r H_m$) decreased slightly to (−17.7 ± 0.5) kJ mol^{-1}, but the entropy ($\Delta_r S_m$) increased by 0.5 J mol^{-1} K^{-1} to 23.0 J mol^{-1} K^{-1}. Otherwise, only $\Sigma\beta^0_{\pm I}$ and $\Sigma\beta^1_{\pm I}$ significantly diverged from their initial values given in Figure 4.

Table 5. Normalization of the Reaction Enthalpy and Entropy with the Pitzer Ion-Interaction Summations ($\Sigma\beta^0_{\pm}$, $\Sigma\beta^1_{\pm}$, β^1_{salt})[a] Based on the Whole Database

	T/K					
	280	288	298	305	313	323
log K°	4.496	4.404	4.297	4.226	4.149	4.058
$\Sigma\beta^0_{\pm}$	−0.083	−0.217	−0.385	−0.502	−0.637	−0.804
$\Sigma\beta^1_{\pm}$	−4.864	−4.726	−4.554	−4.433	−4.296	−4.123
β^1_{salt}	−2.619	−2.619	−2.619	−2.619	−2.619	−2.619
AAE	0.031	0.028	0.065	0.055	0.035	0.046
AAE − $AAE_{Tab.3}$	+0.005	+0.002	+0.028	+0.021	+0.006	+0.006

[a] $\Sigma\beta^0_{\pm} = -0.017T/\mathrm{K} + 4.61$. $\Sigma\beta^1_{\pm} = 0.017T/\mathrm{K} - 9.69$. $\beta^1_{salt} = -2.62$. $\Delta_r H_m = (-17.7 \pm 0.5)$ kJ mol^{-1}. $\Delta_r S_m = 23.0$ J mol^{-1} K^{-1}.

Conclusions

The thermodynamic equilibrium constant (K°) for the $Fe^{3+}CDTA^{4-} + OH^- \rightleftarrows Fe^{3+}OH^-CDTA^{4-}$ complex-formation reaction was evaluated by means of measured concentrations and calculations of activity coefficient quotients in NaCl electrolytic solutions of (1.5×10^{-4} to 0.95) mol kg^{-1} ionic strength. The variation of temperature (280 to 323 K) allowed the estimation of the reaction enthalpy ($\Delta_r H_m$) and entropy ($\Delta_r S_m$), which were determined to be (−17.7 ± 0.5) kJ mol^{-1} and 23.0 J mol^{-1} K^{-1}, respectively. This was achieved in conjunction with the Hückel, Bromley, Scatchard, and Pitzer $\gamma_{\pm}$ predictions. It was also determined that most of the models' ion-interaction empirical values (ϵ, Huckel; B_1, B_2, Bromley; C_1, C_2, C_3, Scatchard; β^1_{salt}, Pitzer) are temperature-independent variables within the studied range. The only exceptions involve Pitzer's ion-interaction summations ($\Sigma\beta^0_{\pm}$, $\Sigma\beta^1_{\pm}$) where a slight but definite linear trend was observed as a function of temperature. Following the normalization procedure, an assessment of the quality of fit between log K_m and log K° − log $\gamma_{\pm}$ based on individual activity coefficient models gave the following results: Hückel (AAE = 0.038 ± 0.014 for I_m < 0.25 mol kg^{-1}), Bromley (AAE = 0.062 ± 0.014 for I_m < 0.95 mol kg^{-1}), Scatchard (AAE = 0.055 ± 0.012 for I_m < 0.95 mol kg^{-1}), and Pitzer (AAE = 0.043 ± 0.015 for I_m < 0.95 mol kg^{-1}).

Literature Cited

(1) Wubs, H. J.; Beenackers, A. C. M. Kinetics of H_2S absorption into aqueous ferric solutions of EDTA and HEDTA. *AIChE J.* **1994**, *40*, 433−444.
(2) Demminck, J. F.; Beenackers, A. C. M. Gas Desulfurization with Ferric Chelates of EDTA and HEDTA: New Model for the

Oxidative Absorption of Hydrogen Sulfide. *Ind. Eng. Chem. Res.* **1998**, *37*, 1444−1453.
(3) Martell, A. E.; Motekaitis, R. J.; Chen, D.; Hancock, R. D.; McManus, D. Selection of new Fe(III)/Fe(II) chelating agents as catalysts for the oxidation of hydrogen sulfide to sulfur by air. *Can. J. Chem.* **1996**, *74*, 1872−1879.
(4) Philip, C. V.; Brooks, D. W. Iron(III) Chelate Complexes of Hydrogen Sulfide and Mercaptans in Aqueous Solution. *Inorg. Chem.* **1974**, *13*, 384−386.
(5) Holbrook, D. L. In *Handbook of Petroleum Refining Processes*, 2nd ed.; Meyers, R. A., Ed.; McGraw-Hill: New York, 1996.
(6) Iliuta, I.; Larachi, F. Concept of bifunctional redox iron-chelate process for H_2S removal in pulp and paper atmospheric emissions. *Chem. Eng. Sci.* **2003**, *58*, 5305−5314.
(7) Smith, R. M.; Motekaitis, R. J.; Martell, A. E. Prediction of stability constants. I. Protonation constants of carboxylates and formation constants of their complexes with class A metal ions. *Inorg. Chim. Acta* **1985**, *99*, 207−216.
(8) Smith, R. M.; Motekaitis, R. J.; Martell, A. E. Prediction of stability constants. II. Metal chelates of natural alkyl amino acids and their synthetic analogues. *Inorg. Chim. Acta* **1985**, *103*, 73−82.
(9) Martell, A. E.; Motekaitis, R. J.; Chen, D.; Hancock, R. D.; McManus, D. Selection of new Fe(III)/Fe(II) chelating agents as catalysts for the oxidation of hydrogen sulfide to sulfur by air. *Can. J. Chem.* **1996**, *74*, 1872−1879.
(10) Piché, S.; Grandjean, B.; Larachi, F. Acid−Base Equilibrium Constants for Ferric *trans*-1,2-Diaminocyclohexanetetraacetic Acid ($Fe^{3+}CDTA^{4-}$/$Fe^{3+}OH^{-}CDTA^{4-}$) in NaCl, Na_2SO_4, and LiCl Aqueous Solutions at 298 K. *J. Chem. Eng. Data* **2003**, *48*, 1578−1582.
(11) Zemaitis, J. F., Jr.; Clark, D. M.; Rafal, M.; Scrivner, N. C. *Handbook of Aqueous Electrolyte Thermodynamics*; American Institute of Chemical Engineers: New York, 1986.
(12) Alonso, P.; Barriada, P.; Rodriguez, I.; Sastre de Vicente, M. E. Acid−Base Equilibrium Constants for Glycine in $NaClO_4$, KCl, and KBr at 298 K. Dependence on Ionic Strength. *J. Chem. Eng. Data* **1998**, *43*, 876−879.
(13) Bromley, L. A. Approximate individual ion values of β in extended Debye−Hückel theory for uni-univalent aqueous solutions at 298.15 K. *J. Chem. Thermodyn.* **1972**, *4*, 669−675.
(14) Bromley, L. A. Thermodynamic properties of strong electrolytes in aqueous solutions. *AIChE J.* **1973**, *19*, 313−317.
(15) Scatchard, G. Osmotic Coefficients and Activity Coefficients in Mixed Electrolyte Solutions. *J. Am. Chem. Soc.* **1961**, *83*, 2636−2642.
(16) Brandaritz, I.; Fiol, S.; Herrero, R.; Vilarino, T.; Sastre de Vicente, M. Protonation Constants of α-Alanine, γ-Aminobutyric Acid, and ϵ-Aminocaproic Acid. *J. Chem. Eng. Data* **1993**, *38*, 531−533.
(17) Pitzer, K. S. Thermodynamics of Electrolytes. I. Theoretical Basis and General Equations. *J. Phys. Chem.* **1973**, *77*, 268−276.
(18) *Activity Coefficients in Electrolyte Solutions*; Pitzer, K. S., Ed.; CRC Press: Boca Raton, FL, 1991; Chapter 3.
(19) Bradley, D. J.; Pitzer, K. S. Thermodynamics of Electrolytes. 12. Dielectric Properties of Water and Debye−Hückel Parameters to 350 °C and 1 kbar. *J. Phys. Chem.* **1979**, *83*, 1599−1603.
(20) Harrison, R. M.; de Mora, S. J.; Rapsomanikis, S.; Johnson, W. R. *Introductory Chemistry for the Environmental Sciences*; Cambridge University Press: New York, 1991.
(21) Gustafson, R. L.; Martell, A. E. Hydrolytic Tendencies of Ferric Chelates. *J. Phys. Chem.* **1963**, *67*, 576−582.

Received for review October 5, 2004. Accepted January 31, 2005. Financial support from the Natural Sciences and Engineering Research Council of Canada (NSERC) and the Fonds Québécois de la Recherche sur la Nature et les Technologies is gratefully acknowledged.

JE049647F